Int. J. Heat Mass Transfer. Vol. 2, pp. 69–82. Pergamon Press 1961. Printed in Great Britain.

THE TWO PHASE BOUNDARY LAYER IN LAMINAR FILM CONDENSATION

J. C. Y. KOH,* E. M. SPARROW and J. P. HARTNETT
Heat Transfer Laboratory, Department of Mechanical Engineering, University of Minnesota, Minneapolis, Minnesota

(*Received* 25 *April* 1960 *and in revised form* 11 *August* 1960)

Abstract—Consideration is given to the two-phase flow problem in laminar film condensation which arises when induced motions of the vapor are included. The shear forces at the liquid–vapour interface, heretofore neglected, have been fully taken into account. It is shown that the problem can be formulated as an exact boundary layer solution. From numerical solutions of the governing equations, it is found that the effects of the interfacial shear on heat transfer are negligible for Prandtl numbers of ten or greater and are quite small even for a Prandtl number of one. For the liquid metal range, the interfacial shear was found to cause substantial reductions in heat transfer.

Résumé—On considère le problème de l'écoulement à deux phases qui se pose, dans la condensation en film laminaire, quand il existe des courants induits de vapeur. On a pleinement tenu compte des forces de frottement sur l'interface vapeur–liquide, jusqu'ici négligées. On a montré que la formulation de ce problème pouvait se faire comme une solution exacte de couche limite. On a trouvé, à partir des solutions numériques des principales équations, que les effets du frottement interfacial sur la transmission de chaleur étaient négligeables pour des nombres de Prandtl égaux ou supérieurs à 10 et étaient encore très petits pour des nombres de Prandtl égaux à 1. Pour les métaux liquides, on a trouvé que le frottement interfacial réduisait de façon substantielle la transmission de chaleur.

Zusammenfassung—Für die laminare Filmkondensation wird das Problem des Zweiphasenstroms behandelt, bei dem zusätzliche Dampfbewegungen auftreten. Die bisher vernachlässigten Schubkräfte an der Trennfläche von Flüssigkeit und Dampf sind dabei voll berücksichtigt. Man kann das Problem als eine exakte Grenzschichtlösung darstellen. Numerische Lösungen der massgebenden Gleichungen zeigen, dass der Einfluss des Schubs an der Trennfläche für den Wärmeübergang vernachlässigbar ist bei Prandtl-Zahlen von zehn und grösser und noch ziemlich klein ist bei einer Prandtl-Zahl von eins. Im Bereich der flüssigen Metalle wird durch den Schub an der Trennfläche der Wärmeübergang beträchtlich herabgesetzt.

Аннотация—В статье обсуждаются вопросы теплообмена двухфазного потока при ламинарной плёночной конденсации, которая возникает при вынужденном движении пара. Учитывается напряжение трения на поверхности раздела жидкости и пара, которые прежде не принимались во внимание. Показано, что эта задача может быть сведена к точному решению пограничного слоя. Исходя из числовых решений основных уравнений найдено, что влияния межповерхностных сил трения на теплообмен незначительны для чисел Прандтля порядка десяти или больше, ничтожно мало для чисел Прандтля порядка единицы. Для ряда жидких металлов найдено, что межповерхностные силы трения вызывают существенное уменьшение теплообмена.

NOMENCLATURE

c_L, c_v, dimensional constants, equations (10) and (17);
c_p, specific heat at constant pressure;
f, dimensionless velocity variable for vapor, equation (18);
F, dimensionless velocity variable for liquid, equation (11);
$\mathbf{F}$, shear stress vector at the interface;
g, acceleration due to gravity;
h, local heat transfer coefficient, $q/(T_{sat}-T_w)$;
h_{fg}, latent heat of condensation;
$\hat{\mathbf{i}}$, unit vector along the x-direction;
$\hat{\mathbf{j}}$, unit vector along the y-direction;
k, thermal conductivity;
$\hat{\mathbf{n}}$, unit vector normal to the liquid–vapor interface;
Nu_x, local Nusselt number, dimensionless, hx/k;

* Present address, Aero-Space Division, Boeing Airplane Company, Seattle, Washington.

Pr, Prandtl number, dimensionless, $c_p\mu/k$;
q, local heat transfer rate per unit area;
$\hat{\mathbf{t}}$, unit vector tangent to the liquid–vapor interface;
T, temperature;
ΔT, $(T_{sat} - T_w)$;
u, velocity component in x-direction;
u_t, velocity component tangent to the interface;
$\mathbf{U}$, velocity vector at the interface;
v, velocity component in y-direction;
x, co-ordinate measuring distance along plate from the leading edge;
y, co-ordinate measuring distance normal to plate;
δ, thickness of condensate layer;
η, similarity variable, equations (10) and (17);
θ, dimensionless temperature, $(T - T_{sat})/(T_w - T_{sat})$;
μ, absolute viscosity;
ν, kinematic viscosity;
ρ, density;
ψ, stream function.

Subscripts
i, interface;
L, liquid;
sat, saturated;
v, vapor;
w, wall.

Superscript
prime ('), differentiation with respect to η.

INTRODUCTION

LAMINAR film condensation on a vertical plate has been actively studied for many years. The pioneer work was reported by Nusselt [1], who formulated the problem in terms of simple force and heat balances within the condensate film. The effects of inertia forces and energy convection were not taken into account. An improvement on Nusselt's analysis was made by Rohsenow [2]. He included energy convection in the heat balance, while continuing to neglect the inertia forces. More recently, Sparrow and Gregg [3] have reformulated the problem in terms of boundary layer theory, including both convection and inertia. They showed that the effect of the inertia forces on heat transfer was fully negligible for Prandtl numbers of 10 or greater and was quite small even for a Prandtl number of one. For condensation of liquid metals, the inertia forces play an important role in decreasing the heat transfer relative to the Nusselt–Rohsenow prediction.

In the physical model which has been used in previous analyses, it has been usual to suppose that the vapor plays a very passive role. In particular, it has been assumed that there is a zero shear force acting on the condensate at the interface between the liquid and vapor. In reality, the flow of the condensed liquid induces motions within the vapor; and, in turn, the induced vapor flow will affect the velocities in the condensate. This mutual interaction requires simultaneous solution of the flow problem in the liquid and vapor. It is this two-phase flow problem and the associated heat transfer to which consideration will be given here.

A sketch of the physical model and co-ordinate system is given in Fig. 1. The plate surface is

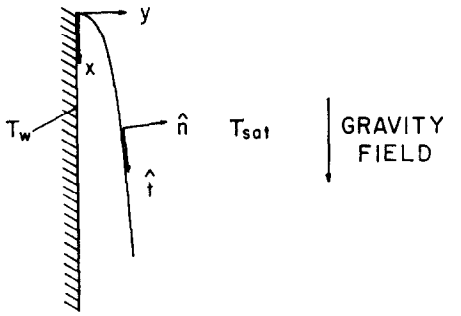

FIG. 1. Physical model and co-ordinates.

maintained at a uniform temperature T_w, while the vapor is pure and saturated at its temperature $T_{sat}(T_{sat} > T_w)$. It will be shown that the problem can be formulated as an exact boundary layer solution.* Numerical results will be reported for Prandtl numbers in the range from 0·003 to 810.

It is interesting to speculate about the expected effects of including interfacial shear forces in the problem. In previous work where the interfacial

* The case of superheated vapor can also be treated within the boundary layer framework.

shear was neglected, all the momentum possessed by the liquid layer was retained by it. But, when interfacial shear forces are permitted to act, then a mechanism is provided by which the motions of the liquid can induce vapor velocities. In the process of inducing such a flow, the liquid must give up some of its momentum. So, for a given condensate layer thickness, the average condensate velocity will be lower when interfacial shear is permitted to act. Consequently, there will be a smaller mass flow of condensate. Since the heat transfer is nearly proportional to the mass flow times the latent heat, it is expected that the heat transfer will decrease.

ANALYSIS

Physical Model and Co-ordinates. A schematic diagram of the physical model and co-ordinate system is shown on Fig. 1. An isothermal vertical flat plate is suspended in a large volume of pure vapor. The vapor is at its saturation temperature, T_{sat}. The plate temperature T_w is lower than T_{sat} and therefore condensation occurs on the plate surface. In steady state, there is a continuous laminar film of condensate flowing downward along the plate. Along the liquid–vapor interface, the vapor velocity tangent to the interface is the same as that of the liquid if there is no slip. The vapor velocity approaches zero at some distance away from the interface. Consequently, there simultaneously exist both liquid and vapor boundary layers.

Boundary Layer Equations. The equations expressing conservation of mass, momentum and energy for steady laminar flow in a liquid boundary layer on a vertical plate are as follows [3]:

Liquid:

$$\text{Continuity} \qquad \frac{\partial u}{\partial x} + \frac{\partial v}{\partial y} = 0. \tag{1}$$

Momentum

$$u\frac{\partial u}{\partial x} + v\frac{\partial u}{\partial y} = \frac{g}{\rho}(\rho - \rho_v) + \nu\frac{\partial^2 u}{\partial y^2}. \tag{2}$$

$$\text{Energy} \qquad u\frac{\partial T}{\partial x} + v\frac{\partial T}{\partial y} = \frac{k}{\rho c_p}\frac{\partial^2 T}{\partial y^2}. \tag{3}$$

The variation of the fluid properties has been neglected, and the viscous dissipation term has been omitted from the energy equation since it is negligibly small. All the fluid properties are those of the condensate except ρ_v, which is the density of the vapor.

Next, turning to the vapor, we note that the saturation condition implies that the vapor temperature is essentially constant. Consequently, the energy equation need not be considered,* and only the continuity and momentum equations remain:

Vapor:

$$\text{Continuity} \qquad \frac{\partial u}{\partial x} + \frac{\partial v}{\partial y} = 0. \tag{4}$$

$$\text{Momentum} \qquad u\frac{\partial u}{\partial x} + v\frac{\partial u}{\partial y} = \nu\frac{\partial^2 u}{\partial y^2}. \tag{5}$$

The boundary conditions are:

at $y = 0$ (for liquid phase),

$$u = 0,\ v = 0,\ T = T_w \tag{6}$$

at $y = \delta$ (liquid–vapour interface),
$T = T_{sat}$
u, v and $\partial u/\partial y$ for both the liquid and vapor must be compatible at the interface (7)

as $y \to \infty$ (for vapor phase), $u \to 0$. (8)

Similarity Transformation. The continuity equation can be satisfied by introducing a stream function ψ such that:

$$u = \frac{\partial \psi}{\partial y} \qquad v = -\frac{\partial \psi}{\partial x}. \tag{9}$$

The remaining partial differential equations can be transformed to the corresponding ordinary differential equations by the following similarity transformation:

a. Liquid Layer

$$\eta_L = \frac{c_L y}{x^{\frac{1}{4}}} \qquad c_L = \left[\frac{g(\rho_L - \rho_v)}{4\nu_L^2\rho_L}\right]^{\frac{1}{4}} \tag{10}$$

* If the vapor is superheated, the energy equation must be used to determine the temperature distribution in the vapor.

Then there is introduced a dimensionless stream function F which is a function of η alone,

$$\psi_L = 4\nu_L c_L x^{\frac{3}{4}} F(\eta_L). \tag{11}$$

The transformation from x, y plane to ν_L, η_L plane can be carried out by the following relations:

$$\left(\frac{\partial}{\partial x}\right)_y = \left(\frac{\partial}{\partial x}\right)_{\eta_L} - \frac{\eta_L}{4x}\left(\frac{\partial}{\partial \eta_L}\right)_x,$$

$$\left(\frac{\partial}{\partial y}\right)_x = \frac{c_L}{x^{\frac{1}{4}}}\left(\frac{\partial}{\partial \eta_L}\right)_x$$

and the velocity components can be expressed in terms of the new variables as follows

$$u = 4\nu_L c_L^2 x^{\frac{1}{2}} F' \tag{12}$$

$$v = \nu_L c_L x^{-\frac{1}{4}} (\eta_L F' - 3F) \tag{13}$$

where the primes denote differentiation with respect to η_L. With this, the momentum and energy equations for the liquid layer are then transformed to the ordinary differential equations:

Momentum
$$F''' + 3FF'' - 2(F')^2 + 1 = 0 \tag{14}$$

Energy
$$\theta'' + 3PrF\theta' = 0 \tag{15}$$

where
$$\theta(\eta_L) = \frac{T - T_{\text{sat}}}{T_w - T_{\text{sat}}}. \tag{16}$$

It may be noted that the momentum equation is independent of the energy equation, and hence, can be solved separately provided certain compatibility conditions at the interface are satisfied.

b. Vapor Layer:

Parallel to the above transformation, the following substitution will be used to reduce the vapor-layer partial-differential equation to an ordinary differential equation:

$$\eta_v = \frac{c_v y}{x^{\frac{1}{4}}} \qquad c_v = \left[\frac{g}{4\nu_v^2}\right]^{\frac{1}{4}} \tag{17}$$

$$\psi_v = 4\nu_v c_v x^{\frac{3}{4}} f(\eta_v) \tag{18}$$

where f is assumed to be a function of η_v only. The resulting ordinary differential equation corresponding to equation (5) is:

Momentum
$$f''' + 3ff'' - 2(f')^2 = 0 \tag{19}$$

The boundary conditions at the interface will now be discussed in some detail.

Interface Matching. It is clear that the velocity, mass transfer and shear force along the interface must be matched in both liquid and vapor phases in such a way that the physical laws are satisfied.* These compatibility requirements will be treated one at a time.

(a) Interface Velocity: Along the liquid–vapor interface, the vapor and liquid velocities tangent to the interface must be equal if there is no slip, i.e.,

$$(u_t)_L = (u_t)_v$$

where t denotes the direction tangent to the interface.

The normal and tangent unit vectors respectively at the interface are:

$$\hat{\mathbf{n}} = (\hat{\mathbf{j}}dx - \hat{\mathbf{i}}d\delta)/(dx^2 + d\delta^2)^{\frac{1}{2}}$$
$$\mathbf{t} = (\hat{\mathbf{i}}dx + \hat{\mathbf{j}}d\delta)/(dx^2 + d\delta^2)^{\frac{1}{2}}$$

The vector velocity at the interface is:

$$\mathbf{U} = \hat{\mathbf{i}}u + \hat{\mathbf{j}}v$$

Hence, the velocity tangent to the interface is:

$$u_t = \mathbf{U} \cdot \hat{\mathbf{t}} = \left(u + v\frac{d\delta}{dx}\right) dx/(dx^2 + d\delta^2)^{\frac{1}{2}} \approx$$
$$\approx u dx/(dx^2 + d\delta^2)^{\frac{1}{2}}$$

The last expression is within the accuracy of the boundary layer assumptions since u is of order one, while v and $d\delta/dx$ are of order δ. Consequently, the no slip condition at the interface is fulfilled if the u velocity components in the liquid and vapor are equal, i.e.,

$$(u_v)_i = (u_L)_i \tag{20}$$

where the subscript i denotes conditions at the interface.

In terms of the transformed variables, this becomes

$$f_i' = F_i' \left[\frac{\rho_L - \rho_v}{\rho_L}\right]^{\frac{1}{4}}$$

* Similar matching conditions were considered in Ref. 5.

and, when $\rho_L \gg \rho_v$

$$f_i' = F_i'. \tag{21}$$

This last form is valid if the vapor pressure is small in comparison to the critical pressure. In the present analysis, it will be assumed that this is the case.

(b) Interface Mass Flow: By continuity, the mass transfer from the vapor to the interface must equal the mass transfer from the interface to the liquid. The mass transfer across the interface can be expressed as :

$$\rho(\mathbf{U} \cdot \hat{\mathbf{n}}) = (\rho v \mathrm{d}x - \rho u \mathrm{d}\delta)/(\mathrm{d}x^2 + \mathrm{d}\delta^2)^{\frac{1}{2}}$$

Therefore, mass conservation requires the following equation to be satisfied at the interface:

$$\left(\rho v - \rho u \frac{\mathrm{d}\delta}{\mathrm{d}x}\right)_{v,i} = \left(\rho v - \rho u \frac{\mathrm{d}\delta}{\mathrm{d}x}\right)_{L,i}. \tag{22}$$

After introducing the new variables, equation (22) takes the form

$$f_i = \left[\frac{(\rho\mu)_L}{(\rho\mu)_v}\right]^{\frac{1}{2}} \left[\frac{\rho_L - \rho_v}{\rho_L}\right]^{\frac{1}{2}} F_i$$

or

$$f_i \approx \left[\frac{(\rho\mu)_L}{(\rho\mu)_v}\right]^{\frac{1}{2}} F_i, \qquad \text{when } \rho_L \gg \rho_v. \tag{23}$$

(c) Interface Shear Stress: According to Newton's Third Law, the force exerted on the liquid by the vapor must be equal to the force exerted on the vapor by the liquid. The total shear stress in Newtonian flow is:

$$\mathbf{F} = \hat{\mathbf{i}}\mu\left(\frac{\partial u}{\partial y} + \frac{\partial v}{\partial x}\right) + \hat{\mathbf{j}}\mu\left(\frac{\partial u}{\partial y} + \frac{\partial v}{\partial x}\right)$$

So, the shear stress tangential to the interface is:

$$\mathbf{F} \cdot \hat{\mathbf{t}} = \frac{\mu \mathrm{d}x\left(\frac{\partial u}{\partial y} + \frac{\partial v}{\partial x}\right) + \mu \mathrm{d}\delta\left(\frac{\partial u}{\partial y} + \frac{\partial v}{\partial x}\right)}{(\mathrm{d}x^2 + \mathrm{d}\delta^2)^{\frac{1}{2}}}$$

Within the framework of boundary layer theory, this expression reduces to:

$$\mathbf{F} \cdot \hat{\mathbf{t}} = \mu \frac{\partial u}{\partial y}.$$

Hence, the balance of tangential shear at the interface is expressed by:

$$\left(\mu \frac{\partial u}{\partial y}\right)_{v,i} = \left(\mu \frac{\partial u}{\partial y}\right)_{L,i} \tag{24}$$

In terms of the new variables, equation (24) can be written as:

$$f_i'' = \left[\frac{(\rho\mu)_L}{(\rho\mu)_v}\right]^{\frac{1}{2}} \left[\frac{\rho_L - \rho_v}{\rho_L}\right]^{\frac{1}{2}} F_i''$$

and for $\rho_L \gg \rho_v$, this becomes

$$f_i'' = \left[\frac{(\rho\mu)_L}{(\rho\mu)_v}\right]^{\frac{1}{2}} F_i''. \tag{25}$$

Boundary Conditions. Making use of these matching conditions and of equations (12) and (16) for u and θ, the boundary conditions (6)–(8) may be rephrased as:

For the momentum equations (19) and (14)

$$\eta = 0 \quad \begin{cases} F = 0 \\ F' = 0 \end{cases} \tag{26}$$

$$\eta_L = (\eta_L)_\delta \text{ or } \eta_v = 0^* \quad \begin{cases} f_i = \left[\frac{(\rho\mu)_L}{(\rho\mu)_v}\right]^{\frac{1}{2}} F_i, \quad f_i' = F_i' \\ f_i'' = \left[\frac{(\rho\mu)_L}{(\rho\mu)_v}\right]^{\frac{1}{2}} F_i'' \end{cases} \tag{27}$$

$$\eta_v \to \infty, \qquad f' \to 0. \tag{28}$$

For the energy equation (15)

$$\eta_L = 0, \qquad \theta = 1 \tag{29}$$

$$\eta_L = (\eta_L)_\delta, \qquad \theta = 0. \tag{30}$$

It is seen that the solution of the momentum equation depends upon the dimensionless film thickness $(\eta_L)_\delta$ and on the ratio $[(\rho\mu)_L/(\rho\mu)_v]^{\frac{1}{2}}$. The appearance of the $\rho\mu$ ratio is a new feature of the problem and arises from the consideration of the continuity conditions at the interface. From physical reasoning, it would be expected that when the vapor density and viscosity are very small, the vapor drag would play a minor role. Conversely, the effects of vapor drag should increase as $(\rho\mu)_L/(\rho\mu)_v$ decreases.

* For convenience we choose $\eta_v = 0$ at the interface. This can be done because η_v does not enter into the interface matching equations.

The Parameter $c_{pL}\Delta T/h_{fg}$

The liquid film thickness δ (and hence $\eta_{L\delta}$) is not known *a priori*, but rather, is one of the results of the analysis. Fortunately, as shown in Ref. 3, $\eta_{L\delta}$ can be replaced by the dimensionless group, $c_{pL}\Delta T/h_{fg}$, which contains quantities which would all be known in any physical situation. The relationship between $\eta_{L\delta}$ and $c_{pL}\Delta T/h_{fg}$ is found by invoking an overall energy balance:

$$\int_0^x k_L\left(\frac{\partial T}{\partial y}\right)_{y=0} dx = \int_0^\delta h_{fg}\rho_L u dy + \int_0^\delta \rho_L u c_{pL}(T_{sat} - T) dy \quad (31)$$

The left-hand side is the heat transferred from the condensate to the plate over a length from $x = 0$ to $x = x$. The first term on the right-hand side is the latent heat of condensation and the last term is the heat liberated by sub-cooling of the liquid. In terms of the new variables, equation (31) becomes:

$$\frac{c_{pL}\Delta T}{h_{fg}} = -3Pr_L\frac{F_i}{\theta_i'} \quad (32)$$

where θ_i' and F_i are the values of $d\theta/d\eta_L$ and F at $\eta_{L\delta}$. The energy equation (15) has been used in obtaining the above relation. For any given Pr_L and $[(\rho\mu)_L/(\rho\mu)_v]^{\frac{1}{2}}$, F_i and θ_i depend only on $\eta_{L\delta}$. Hence, there is a unique relation* between the liquid layer thickness $\eta_{L\delta}$ and $c_{pL}\Delta T/h_{fg}$. The present problem therefore involves three parameters, namely, Pr_L, $[(\rho\mu)_L/(\rho\mu)_v]^{\frac{1}{2}}$, and $c_{pL}\Delta T/h_{fg}$.

Heat transfer formulas. In the preceding paragraphs, the governing differential equations for the velocity and temperature distributions have been derived. Now, it will be shown how the solutions of these equations are related to the heat transfer results. According to Fourier's Law, the local heat transfer at the surface of the plate is given by

$$q = k_L\left(\frac{\partial T}{\partial y}\right)_{y0} .$$

* In Ref. 3, it was found that $c_{pL}\Delta T/h_{fg}$ increases as the film thickness increases. The same trend applies in the present study.

In terms of the transformed variables of equations (10) and (16) the expression for q becomes

$$q = k_L(T_{sat} - T_w)\left[\frac{g(\rho_L - \rho_v)}{4\rho_L\nu_L^2 x}\right]^{\frac{1}{4}}[-\theta'(0)] \quad (33)$$

where $\theta'(0)$ is an abbreviation for $[d\theta/d\eta]_{\eta=0}$. It is convenient to report the heat transfer results in terms of a local heat transfer coefficient and local Nusselt number defined as follows

$$h = \frac{q}{T_{sat} - T_w} \qquad Nu_x = \frac{hx}{k_L} \quad (34)$$

With this, the heat transfer can be rephrased as

$$Nu_x = \left[\frac{g(\rho_L - \rho_v)x^3}{4\rho_L\nu_L^2}\right]^{\frac{1}{4}}[-\theta'(0)] \quad (35a)$$

or

$$Nu_x\left[\frac{c_{pL}\Delta T/h_{fg}}{gc_{pL}(\rho_L - \rho_v)x^3/4\nu_L k_L}\right]^{\frac{1}{4}} = \left[\frac{c_{pL}\Delta T/h_{fg}}{Pr_L}\right]^{\frac{1}{4}}[-\theta'(0)] \quad (35b)$$

where the last form has been found by experience (Ref. 3, Appendix 1) to provide an especially convenient representation. It is seen from equations (35) that once the dimensionless temperature slope $[-\theta'(0)]$ has been supplied by the solutions, then the heat transfer is immediately known. Since Pr, $c_{pL}\Delta T/h_{fg}$, and $(\rho\mu)_L/(\rho\mu)_v$ appear as parameters in the governing equations, it would appear that $\theta'(0)$ will also depend on these same parameters. It can be shown without difficulty that the *average* heat transfer coefficient is 4/3 times the local coefficient.

Solutions. The velocity and temperature distributions are governed by equations (14), (15), and (19) in conjunction with the boundary conditions (26)–(30). It is not possible to find analytical solutions to this formidable array and hence numerical means were used. The general procedure by which solutions were obtained may be outlined as follows: Consideration was first given to the momentum equations (14) and (19), and a dimensionless film thickness $\eta_{L\delta}$ was selected. Then, a guess was made for the value of F_i' and this, together with the conditions $F(0) = F'(0) = 0$, provided three boundary conditions for the liquid momentum equation

(14). A solution for equation (14) could then be carried out. The values of F_i and F_i' corresponding to this solution can be transformed by equation (27) into values of f_i and f_i', once the ratio $[(\rho\mu)_L/(\rho\mu)_v]^{\frac{1}{2}}$ is assigned. And, with the third condition $f'(\infty) \to 0$, the vapor momentum equation (19) was solved. Finally, it remained to be checked whether Newton's Third Law as expressed by the last of equations (27) was satisfied by the F_i'' and f_i'' values from the liquid and vapor solutions. If not, a new guess was made for F_i' and the entire calculation was repeated until the matching condition for F_i'' and f_i'' was fulfilled. Once a solution of the momentum equations for a given $\eta_{L\delta}$ and $\rho\mu$ ratio was obtained, it was used as input data for the solution of the energy equation (15). Then, for a fixed Prandtl number the heat transfer and the value of $c_{pL}\Delta T/h_{fg}$ were evaluated from equations (35) and (32) respectively.

The actual numerical solutions were carried out by recasting the differential equations into integral form in a manner analogous to Ref. 4, and then iterating each equation until convergence was achieved. The numerical integrations were accomplished by the trapezoidal rule.

For the higher Prandtl number fluids ($Pr \geq 10$), it has already been demonstrated in Ref. 3 that the inertia terms in the liquid momentum equation can be neglected. As a consequence, the solutions for the higher Prandtl numbers can in part be carried out analytically. In the absence of the inertia terms, equation (14) becomes

$$F''' + 1 = 0. \tag{36}$$

A solution of this equation which satisfies the conditions $F(0) = F'(0) = 0$ and $F' = F_i'$ at $\eta_L = \eta_{L\delta}$ is

$$F = \frac{\eta_L^2}{2}\left(C - \frac{\eta_L}{3}\right) \tag{37a}$$

$$F' = C\eta_L - \eta_L^2/2 \tag{37b}$$

$$F'' = -\eta_L + C \tag{37c}$$

where $C = F_i'/\eta_{L\delta} + \eta_{L\delta}/2$.

So, for a given value of the film thickness $\eta_{L\delta}$, the solution for F corresponding to a particular interfacial shear F_i is given in a simple analytical form. The general procedure for simultaneous solution of liquid and vapor remains as previously described.

The cases for which solutions have been carried out are listed in Tables 1 and 2 and may be summarized as follows: For the non-metallic liquids, solutions were obtained for Prandtl numbers between 1 and 810* for $c_{pL}\Delta T/h_{fg}$ ranging from essentially zero to 1·2 and for $[(\rho\mu)_L/(\rho\mu)_v]^{\frac{1}{2}}$ between 10 and 600. For the liquid metals, the solutions were found for Prandtl numbers of 0·003, and 0·008, and 0·03 for $c_{pL}\Delta T/h_{fg}$ ranging from essentially zero to 0·1 and for $[(\rho\mu)_L/(\rho\mu)_v]^{\frac{1}{2}}$ of 100 and 600. The results obtained from these solutions will be presented and discussed in the next section.

HEAT TRANSFER RESULTS

Ordinary liquids ($Pr \geq 1$). The Nusselt numbers which have been calculated from the solution of the governing equations are given in Table 1 and at the top of Table 2 under the designation *interfacial shear*. The results are tabulated as a function of the Prandtl number, $c_{pL}\Delta T/h_{fg}$, and the $(\rho\mu)^{\frac{1}{2}}$ ratio. Also given for comparison purposes are the Nusselt number results which correspond to the condition of no interfacial shear (Ref. 3). The percentage deviation of the earlier results from those of the present analysis is shown. For Prandtl numbers of 10 and above, all solutions were carried out neglecting inertia forces in the liquid layer momentum equation, in accordance with the findings of Ref. 3. Turning first to the results for $Pr = 10$, it is seen that no matter what values of the parameters $[(\rho\mu)_L/(\rho\mu)_v]^{\frac{1}{2}}$ and $c_{pL}\Delta T/h_{fg}$ are selected, the effect of the interfacial shear on the Nusselt number is very small. The greatest deviation of 1·1 $\sim$ 1·3 per cent occurs at a $c_{pL}\Delta T/h_{fg}$ of 1·2, which is usually outside the range of current practice. It may also be observed that varying the $(\rho\mu)^{\frac{1}{2}}$ ratio from 10 to 600 has a negligible effect on the Nusselt number. On the other hand, increasing the thickness of the condensate layer (i.e., increasing $\eta_{L\delta}$) causes the interfacial drag to be somewhat more effective in reducing the heat transfer. With increasing Prandtl number, the value of the dimensionless film thickness $\eta_{L\delta}$ *decreases* at a fixed $c_{pL}\Delta T/h_{fg}$ (columns 3 and

* A computationally convenient number.

Table 1. Summary of Results. No Inertia Terms in Momentum Equation of Condensate Layer

Pr_L	$[(\rho\mu)_L/(\rho\mu)_v]^{\frac{1}{2}}$	$c_{pL}\Delta T/h_{fg}$	$\eta_{L\delta}$	$Nu_x[c_{pL}\Delta T/h_{fg} \times 4\nu_L^2 k_L/gc_{pL}(\rho_L - \rho_v)x^3]^{\frac{1}{4}}$		
				Interfacial shear	No shear	Per cent deviation
810	600	0·08282	0·1	1·014	1·014	0
810	10	0·08275	0·1	1·014	1·014	0
810	600	1·294	0·1867	1·175	1·175	0
810	10	1·290	0·1867	1·174	1·174	0
10	600	0·08232	0·3	1·012	1·013	0·1
10	100	0·08224	0·3	1·012	1·014	0·2
10	10	0·08191	0·3	1·011	1·014	0·3
10	150	0·2694	0·4	1·039	1·043	0·38
10	10	0·2679	0·4	1·037	1·042	0·48
10	10	0·7021	0·5	1·091	1·102	1·0
10	600	1·196	0·56	1·147	1·161	1·2
10	150	1·197	0·56	1·147	1·161	1·2
10	10	1·185	0·56	1·145	1·159	1·2
1	600	0·07833	0·5335	0·999	1·013	1·4
1	10	0·07778	0·5335	0·998	1·013	1·5
1	600	0·8369	0·9958	1·031	1·119	8·5
1	10	0·8316	0·9958	1·029	1·118	8·6

Table 2. Summary of Results. Including Inertia Terms in Momentum Equation of Condensate Layer

Pr_L	$[(\rho\mu)_L/(\rho\mu)_v]^{\frac{1}{2}}$	$c_{pL}\Delta T/h_{fg}$	$\eta_{L\delta}$	$Nu_x[c_{pL}\Delta T/h_{fg} \times 4\nu_L^2 k_L/gc_{pL}(\rho_L - \rho_v)x^3]^{\frac{1}{4}}$				
				Interfacial shear	No shear	Per cent Deviation	No shear, no inertia	Per cent deviation
1	600	0·07704	0·5335	0·9951	1·010	1·5	1·013	1·8
1	600	0·3447	0·8	0·9893	1·037	4·9	1·054	6·5
1	10	0·3430	0·8	0·9878	1·036	4·9	1·054	6·7
1	600	0·5231	0·9	0·9909	1·054	6·4	1·079	8·9
1	600	0·7478	0·9958	0·9967	1·075	7·8	1·108	11·2
1	10	0·7442	0·9958	0·9953	1·075	8·0	1·108	11·3
0·03	600	$4·79 \times 10^{-5}$	0·2	0·9995	1	0		
0·03	600	$2·41 \times 10^{-4}$	0·3	0·9979	1	0·2		
0·03	600	$1·774 \times 10^{-3}$	0·5	0·9864	0·997	1·1		
0·03	600	$9·499 \times 10^{-3}$	0·8	0·9386	0·9822	4·6		
0·03	600	0·03215	1·2	0·8510	0·9512	11·8		
0·03	600	0·06831	1·6	0·7741	0·910	17·5		
0·03	600	0·1487	2·2	0·7100				
0·008	600	$4·728 \times 10^{-4}$	0·5	0·9862	0·998	1·2		
0·008	600	$5·059 \times 10^{-3}$	1·0	0·8923	0·967	8·4		
0·008	600	0·01526	1·5	0·7849	0·911	16		
0·008	600	0·06579	2·8	0·6110	0·767	25·5		
0·008	100	0·06577	2·8	0·6109	0·767	25·5		
0·008	600	0·1012	3·4	0·5639	0·713	26·4		
0·003	600	$7·497 \times 10^{-5}$	0·4	0·9940	1	0·6		
0·003	600	$1·907 \times 10^{-3}$	1·0	0·8931	0·967	8·5		
0·003	600	$8·927 \times 10^{-3}$	1·8	0·7305	0·8742	19·7		
0·003	600	0·02828	3·0	0·5867	0·740	26·1		
0·003	600	0·08746	5·0	0·4722	0·5995	27		

4 of the table). So, it would be expected that the effects of vapor drag would decrease as Prandtl number increases. This is clearly indicated by the results for $Pr = 810$, which show no deviations (to four figures) from those based on zero vapor drag. From these findings, it may be inferred that the interfacial shear is indeed very nearly zero for the high Prandtl number fluids, and this will be verified later when the velocity distributions are shown.

Inasmuch as interfacial shear is practically unimportant for $Pr \geqslant 10$, the Nusselt number results of Ref. 3 have been accepted without numerical alteration and have been rephrased and replotted on the more convenient coordinates of Fig. 2.

higher Prandtl numbers. For example, for $c_{pL}\Delta T/h_{fg} = 0{\cdot}75$, the Nusselt number is reduced by 8 per cent when interfacial shear is taken into account. If the comparison were made using the non-inertia result of Ref. 3 as a basis, then the present Nusselt number would be 11 per cent low. Further study of the $Pr = 1{\cdot}0$ results shows that the value of the $\rho\mu$ ratio again appears to be a second order effect within the range considered here. From this, we are led to speculate that there must be a threshold value above which the magnitude of the $\rho\mu$ ratio is unimportant, and further, that this threshold lies below most of the technically interesting situations.

The Nusselt number results for $Pr = 1{\cdot}0$ as listed in Table 2 have been plotted on Fig. 2

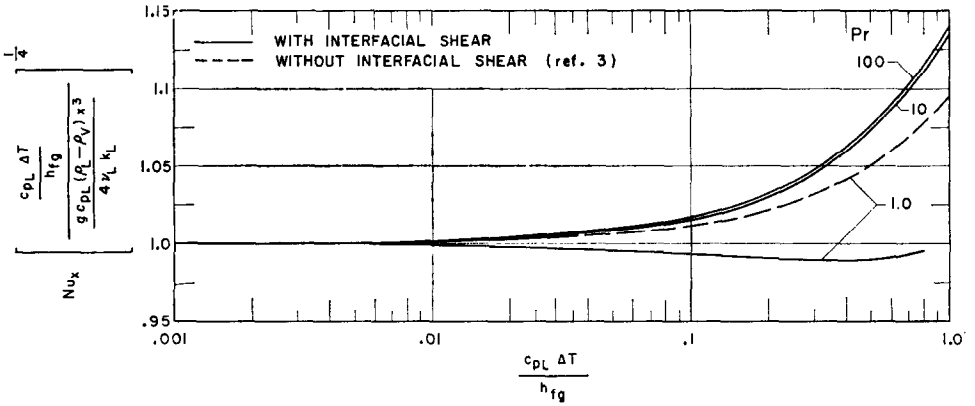

FIG. 2. Effect of interfacial shear stress on heat transfer, $Pr \geqslant 1$.

For a Prandtl number of 1·0, the inertia forces continue to be unimportant for thin condensate films (small $c_{pL}\Delta T/h_{fg}$) and have a small effect for thicker films [3]. So, with this in mind, solutions including the effects of interfacial shear were obtained both with and without inertia forces. The Nusselt number results without inertia are given at the end of Table 1, while those including inertia appear at the beginning of Table 2. In each table are included for comparison purposes the appropriate results of Ref. 3. An additional comparison is made in Table 2 where the non-inertia results of Ref. 3 are given as well as those including inertia. Inspection of the tables shows that the effects of interfacial shear are much greater for $Pr = 1{\cdot}0$ than for the

as a solid curve. Also included in the figure is a dashed curve depicting the results for zero interfacial shear. Without interfacial shear, the curve rises monotonically with increasing film thickness; while with interfacial shear, the curve drops slightly at first and then commences to rise. This behavior may not seem unreasonable when the various factors effecting the heat transfer are discussed. First of all, for very thin films (small $c_{pL}\Delta T/h_{fg}$) neither the inertia forces nor the interfacial shear nor the sub-cooling are significant, and all curves come back to a common asymptote of unity. Now, as the film thickness increases, the inertia forces and interfacial shear tend to decrease the heat transfer, while the sub-cooling tends to increase the heat transfer.

For $Pr = 1{\cdot}0$ without interfacial shear, the subcooling wins out over the inertia forces and the curve rises. But, when interfacial shear is introduced, the inertia forces are given an ally which appears to be strong enough to win out for thinner films, only to lose to the effects of subcooling for the thicker films.

Liquid metals. The Nusselt number results for the liquid metal range as computed from the solutions of the governing equations including inertia and interfacial shear are given in Table 2. Also given there are the results based on zero interfacial shear. Inspection of the table shows that except for very small values of $c_{pL}\Delta T/h_{fg}$, the effects of interfacial shear are quite large. For example, for $Pr = 0{\cdot}008$ and $c_{pL}\Delta T/h_{fg} = 0{\cdot}06$, the Nusselt number as computed without interfacial shear is 25 per cent too high. As might be expected on the basis of the prior discussion, the effects of interfacial shear increase with decreasing Prandtl number. Almost all the calculations were carried out for a value of $[(\rho\mu)_L/(\rho\mu)_v]^{\frac{1}{2}}$ of 600, which is realistic for liquid metals. As a check, a single case was computed with this ratio reduced to 100, and as seen in Table 2, the Nusselt number is unchanged.

These Nusselt number results for low Prandtl numbers are presented on Fig. 3. The solid curves represent the solutions with interfacial shear and the dashed curves* are without interfacial shear. The figure graphically demonstrates the substantial effects of interfacial shear. From these findings, it may be inferred that the shear at the interface differs appreciably from zero, and this will be convincingly demonstrated in the following section.

VELOCITY AND TEMPERATURE PROFILES

The velocity profiles are of considerable interest since they show the detailed manner in which the flow is affected by the interfacial shear. Space limitations preclude a presentation of results for all the cases studied, so we must content ourselves with showing representative situations. Such a presentation is made on Figs. 4 through 7, which correspond respectively to Prandtl numbers of 10, 1, 0·03 and 0·003. Curves associated with representative values of

* The results of Ref. 3 for $c_{pL}\Delta T/h_{fg} > 0{\cdot}025$ were found to be low by about 1 per cent and corrections have been made.

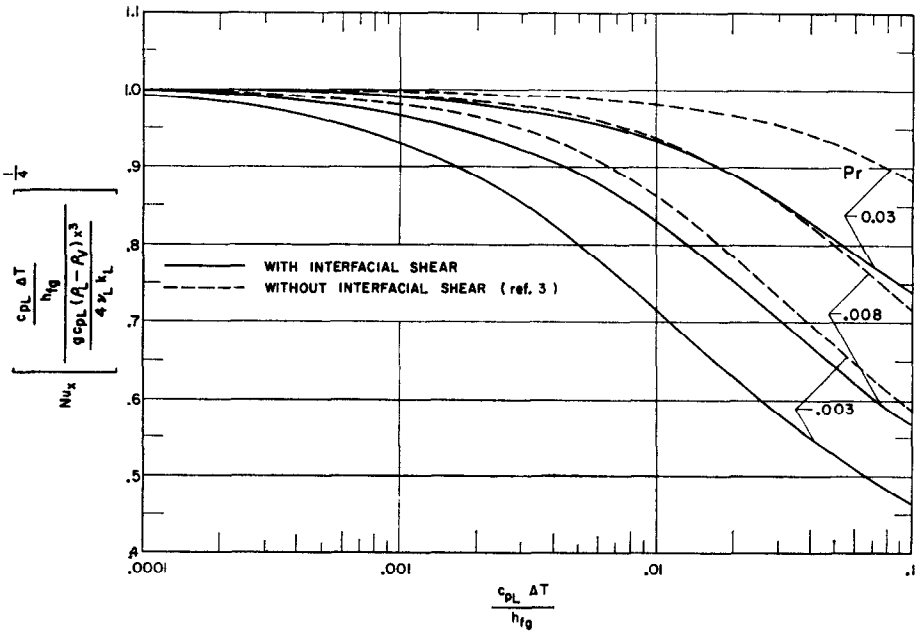

FIG. 3. Effect of interfacial shear stress on heat transfer, liquid metal range.

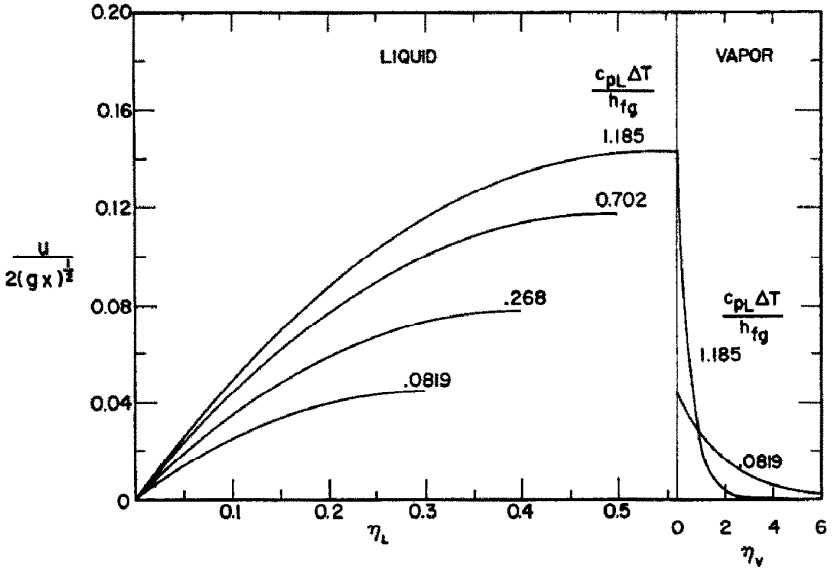

FIG. 4. Velocity profiles, $Pr = 10$, $[(\rho\mu)_L/(\rho\mu)_v]^{\frac{1}{2}} = 10$.

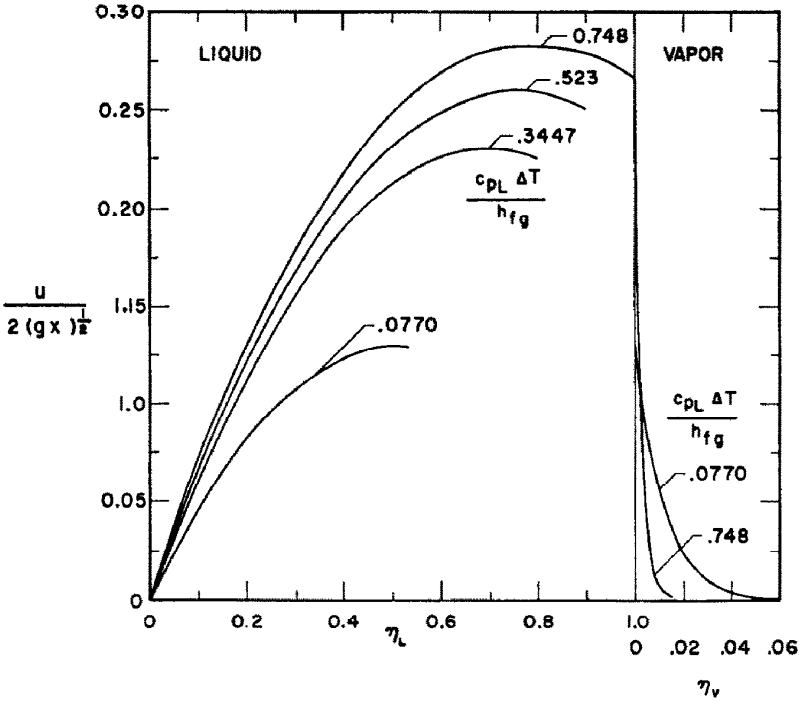

FIG. 5. Velocity profiles, $Pr = 1$, $[(\rho\mu)_L/(\rho\mu)_v]^{\frac{1}{2}} = 600$.

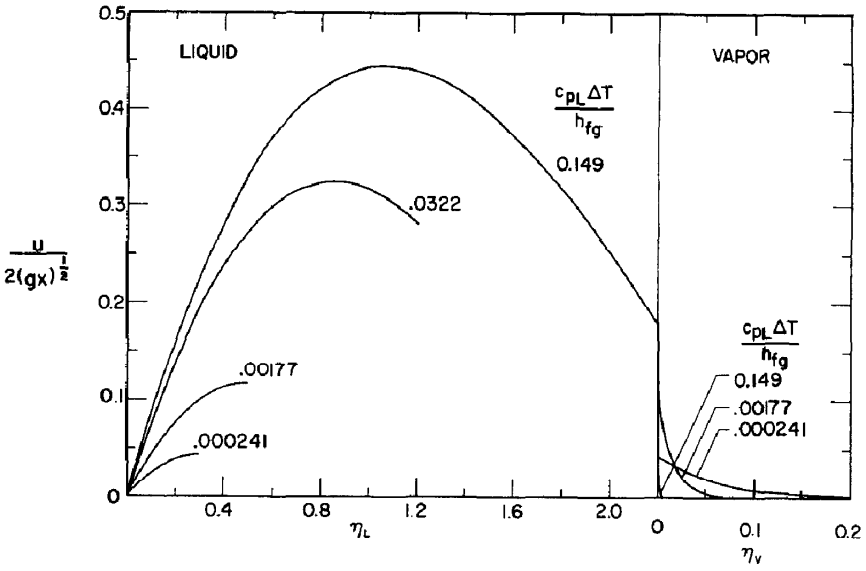

FIG. 6. Velocity profiles, $Pr = 0{\cdot}03$, $[(\rho\mu)_L/(\rho\mu)_v]^{\frac{1}{2}} = 600$.

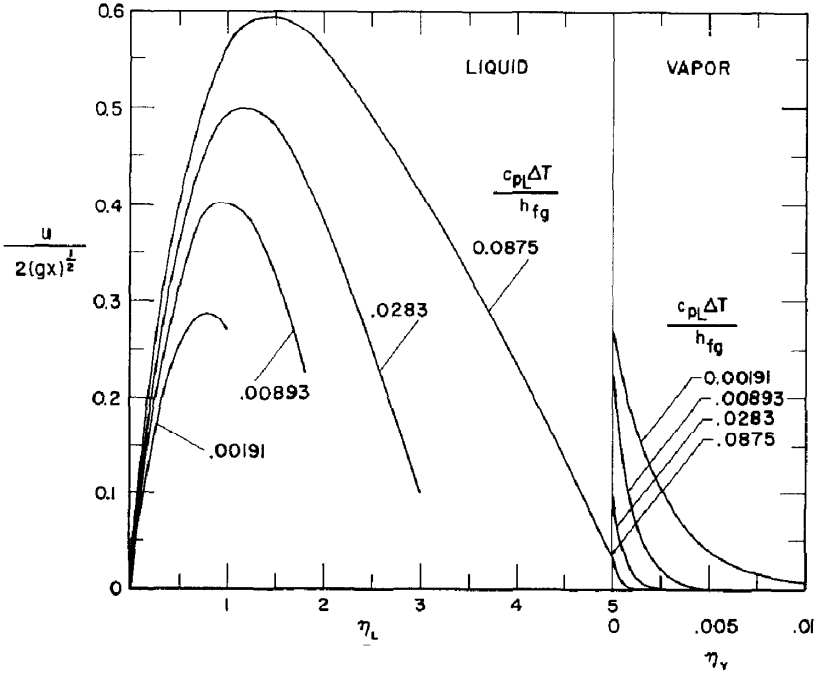

FIG. 7. Velocity profiles, $Pr = 0{\cdot}003$, $[(\rho\mu)_L/(\rho\mu)_v]^{\frac{1}{2}} = 600$.

$c_{pL}\Delta T/h_{fg}$ are shown on each figure. Both liquid and vapor velocities have been plotted; and to facilitate this, the abscissa scale has been subdivided into two parts, the left-hand portion applying to the liquid and the right-hand portion to the vapor. The velocity distribution corresponding to a given value of $c_{pL}\Delta T/h_{fg}$ is made up of the liquid layer curve from the left portion of the figure to which is continuously joined the vapor layer curve from the right portion of the figure. The gap between corresponding liquid and vapor curves is due solely to the method of plotting.

Figs. 6 and 7, which correspond to liquid metal Prandtl numbers. For example, on Fig. 7, cases are shown where the velocity maximum (i.e., the zero shear condition) occurs at a position less than half-way across the film.

The temperature profiles are less informative, and the results may be summarized on two typical Figs., 8 and 9. The first of these corresponds to high Prandtl numbers ($Pr = 10$) and the second to low Prandtl numbers ($Pr = 0{\cdot}003$). Turning to Fig. 8, it may be seen that the temperature profiles for thin films are nearly straight lines, indicating that conduction dominates and

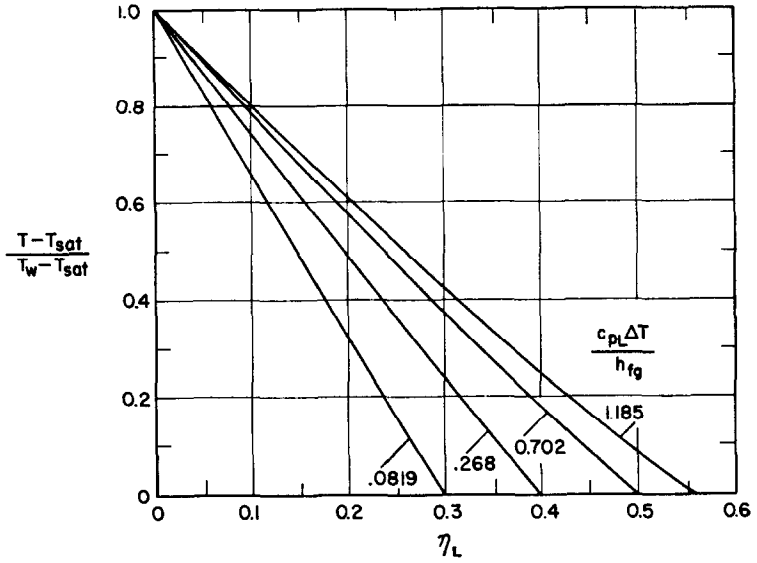

FIG. 8. Temperature profiles, $Pr = 10$, $[(\rho\mu)_L/(\rho\mu)_v]^{\frac{1}{2}} = 10$.

Turning first to Fig. 4, it is easily seen that the curves for the condensate velocity have essentially zero slope at the interface. Since the shear stress is proportional to the slope of the velocity profile, it is apparent that the condition of zero interfacial shear is essentially fulfilled for $Pr = 10$. Next, proceeding to Fig. 5 for $Pr = 1{\cdot}0$, we observe that the condition of zero shear is no longer achieved at the interface, but rather at some location within the liquid film. The thicker the film, the further removed from the interface is the velocity maximum and consequently, the greater the departure from the condition of zero interfacial shear. The effects of interfacial shear are demonstrated even more dramatically on

convection plays a small role. For thicker films, the effect of convection is felt more and more, and the departure from the straight line profile is somewhat greater. For low Prandtl numbers, Fig. 9, the deviations from the straight line profile are not as great as those noted on Fig. 8. This is undoubtedly due to the fact that the liquid metals have very high heat conductivities.

CONCLUDING REMARKS

It has been shown that the two-phase flow problem which arises in laminar film condensation when the induced vapor motion is included can be formulated as an exact boundary layer solution. It is found that the effect on the heat

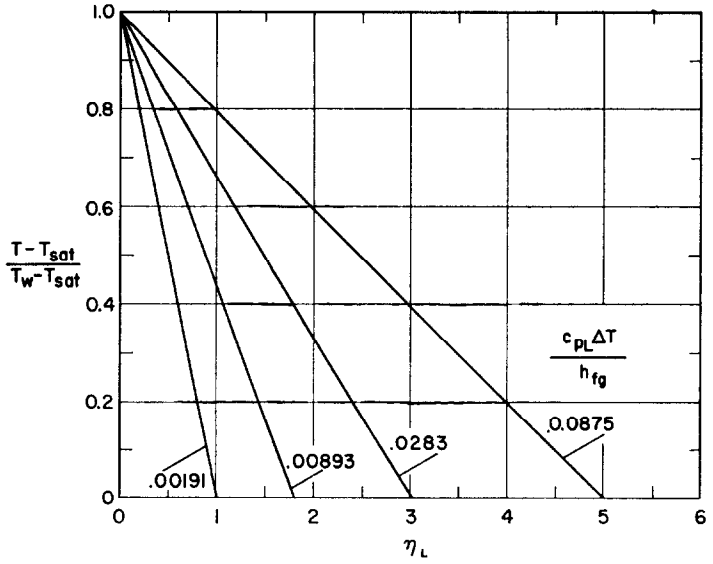

FIG. 9. Temperature profiles, $Pr = 0{\cdot}003$, $[(\rho\mu)_L/(\rho\mu)_v]^{\frac{1}{2}} = 600$.

transfer of the heretofore-neglected shear at the liquid–vapor interface is negligible for Prandtl numbers of ten and higher and is quite small even for a Prandtl number of one. For the condensation of liquid metals, the interfacial shear does cause a substantial reduction of the heat transfer. For all Prandtl numbers, it was found that the effect of the interfacial shear on the heat transfer increased with film thickness (i.e., increased $c_{pL}\Delta T/h_{fg}$). On the other hand, the heat transfer was relatively unaffected by the magnitude of the parameter $[(\rho\mu)_L/(\rho\mu)_v]^{\frac{1}{2}}$.

It is interesting to observe that in the case of film boiling, the governing equations are the same as those derived here, except that the role of liquid and vapor are interchanged. So, the jump of the velocity functions at the interface is governed by $[(\rho\mu)_v/(\rho\mu)_L]^{\frac{1}{2}}$, rather than the reciprocal as appears in the condensation problem. This "jump parameter" will be substantially less than unity. Since the present investigation considered values of the "jump parameter" no less than 10, the present solutions cannot be applied to film boiling without further verification.

REFERENCES

1. W. NUSSELT, *Z. Ver. Deutsch. Ing.*, **60**, 541 and 569 (1916).
2. W. M. ROHSENOW, *Trans. Amer. Soc. Mech. Engrs*, **78**, 1645 (1956).
3. E. M. SPARROW and J. L. GREGG, *J. Heat Transfer*, Series C, *Trans. Amer. Soc. Mech. Engrs*, **81**, 13, (1959).
4. A. A. HAYDAY, *Proceedings, 1959 Heat Transfer and Fluid Mechanics Institute*, pp. 156–170. Stanford University Press, Stanford, California (1959).
5. S. M. SCALA and G. W. SUTTON, *Proceedings, 1958 Heat Transfer and Fluid Mechanics Institute*, pp. 231–240. Stanford University Press, Stanford, California (1958).